remote sensing

MDPI

Article

Characteristics and Source Analysis of Ozone Pollution in Tianjin from 2013 to 2022

Shuo Dong [1], Pengfei Ma [2], Xingchuan Yang [1], Nana Luo [3], Linhan Chen [2], Lili Wang [1], Hanyang Song [1], Shaohua Zhao [2] and Wenji Zhao [1,*]

[1] College of Resource Environment and Tourism, Capital Normal University, Beijing 100048, China; 2220902045@cnu.edu.cn (S.D.)
[2] Ministry of Ecology and Environment Center for Satellite Application on Ecology and Environment State Environmental Protection Key Laboratory of Satellite Remote Sensing, Beijing 100094, China
[3] School of Geomatics and Urban Information, Beijing University of Civil Engineering and Architecture, Beijing 100044, China
* Correspondence: 4973@cnu.edu.cn

Abstract: This study has analyzed ozone pollution in Tianjin from 2013 to 2022, focusing on the relationships between ozone distribution, meteorological conditions, and precursor substances. A method for identifying high-value areas of ozone precursors using the Ozone Sensitivity Factor (FNR) has been introduced. Results show that the average ozone concentration in Tianjin has been 100.608 $\mu g/m^3$, with an annual growth rate of 2.84 $\mu g \cdot m^{-3} \cdot yr^{-1}$. Tianjin has ranked among the top provinces and urban agglomerations in China for both ozone concentration and growth rate. Ozone levels have peaked in summer, followed by spring, autumn, and winter, while the growth rate has been highest in spring. This indicates that ozone pollution extends from summer into spring and autumn. An analysis of six ozone pollution events reveals significant regional transmission impacts from northern Hebei and Inner Mongolia, contributing over 30%, with additional significant contributions from southern and southwestern Hebei and western Shandong. In terms of controlling ozone precursors, high-HCHO-value areas have been identified. The correlation between areas of high HCHO values and ground-level ozone concentrations was 0.56339 during the ozone season and 0.2214 during the non-ozone season, both of which improved identification accuracy to varying degrees, suggesting that targeting precursor emissions in these areas could enhance pollution mitigation efforts.

Keywords: ozone pollution; ozone source; Tianjin; high-value area identification

check for updates

Citation: Dong, S.; Ma, P.; Yang, X.; Luo, N.; Chen, L.; Wang, L.; Song, H.; Zhao, S.; Zhao, W. Characteristics and Source Analysis of Ozone Pollution in Tianjin from 2013 to 2022. *Remote Sens.* **2024**, *16*, 3970. https://doi.org/10.3390/rs16213970

Academic Editor: Manuel Antón

Received: 16 September 2024
Revised: 13 October 2024
Accepted: 23 October 2024
Published: 25 October 2024

Copyright: © 2024 by the authors. Licensee MDPI, Basel, Switzerland. This article is an open access article distributed under the terms and conditions of the Creative Commons Attribution (CC BY) license (https://creativecommons.org/licenses/by/4.0/).

1. Introduction

Ozone (O_3) is a crucial atmospheric trace gas [1–4]. In the stratosphere, ozone protects humans and ecosystems by absorbing ultraviolet radiation. However, elevated ground-level ozone in the troposphere can lead to urban photochemical smog [5], This phenomenon adversely affects human health, contributing to respiratory issues such as mucosal irritation, cardiovascular diseases, pneumonia, chronic obstructive pulmonary disease, asthma, allergic rhinitis, and other respiratory conditions [6–10], as well as the growth of plants and crops [11]. In 2022, the national average percentage of days with air quality categorized as excellent and good decreased by 1.0% compared to the previous year. During this period, $PM_{2.5}$ and PM_{10} concentrations remained stable or exhibited a decreasing trend. However, ozone concentrations deteriorated by 5.8% compared to the same period the previous year, indicating it as another significant pollutant, following $PM_{2.5}$, affecting the enhancement and management of urban air quality [12,13].

Many studies have investigated ozone pollution in main cities across China [1,14–21], Ground-based monitoring stations have been constrained by low spatial resolution, which has led to insufficient coverage and monitoring capabilities in remote areas [22]. Satellite

remote sensing has provided continuous access to data with a high spatial and temporal resolution. The CHAP dataset has integrated remote sensing data from multiple sources and employed machine learning techniques to estimate ground-level air pollutant concentrations in China with high resolution and quality. Unlike traditional data sources, the CHAP dataset has comprehensively incorporated the influencing factors of air pollutants. Consequently, studies based on CHAP data have proven to be more reliable and informative, serving as a valuable reference for analyzing the characteristics and sources of ozone pollution in Tianjin from 2013 to 2022 [3]. Tropospheric ozone originates primarily from four sources: (1) stratosphere–troposphere exchange, which involves the downward transport of ozone from the stratosphere [23–26]; (2) photocatalytic reactions of ozone precursors volatile organic compounds (VOCs) and nitrogen oxides (NOx) under sunlight irradiation [27]; (3) the local diffusion and regional transport of ozone and its precursors [5]; (4) diffusion and regional transport [28,29]. However, studies indicate that one of the primary reasons for frequent summer ozone pollution events in the Beijing–Tianjin–Hebei region is regional transport and diffusion caused by meteorological factors [30]. Many scholars use backward trajectory clustering analysis to analyze the sources of pollutants [31]. Another critical factor is the photochemical reactions of local precursors under conditions of high temperature and low humidity [18]. Studies focusing on local ozone production highlight the primary role played by emissions of two major precursors [32–34]. Ozone is also very sensitive to precursor emissions [28,35]. Ozone formation exhibits a nonlinear relationship with precursor emissions, with reductions in nitrogen oxides (NOx) and increases in volatile organic compounds (VOCs) enhancing ground-level ozone concentrations [36]. Since 2013, China has observed a rising trend in volatile organic compound (VOC) emissions, underscoring their sensitivity and impact on ozone levels [37,38].

There is a wide variety of volatile organic compounds (VOCs), and the physicochemical properties of different species vary. HCHO is an intermediate product of VOCs, accounting for 25 to 48 percent of the total atmospheric carbonyl compounds [39,40]. In addition to indirectly affecting photochemical reactions, it also presents some harm to humans [41–43]. HCHO comes from a wide range of sources [44,45]. Many scholars have studied the different urban sources [40,46–49]. Current advancements in satellite remote sensing technology facilitate the measurement of HCHO column concentrations, aiding in VOC monitoring [50].

Recent studies have extensively employed the FNR (formaldehyde-to-nitrogen dioxide ratio retrieved by satellite) index to examine ozone formation sensitivity (OFS) [51]. Ozone formation mechanisms are categorized as NOx-biased control, synergistic control, and VOC-biased control, depending on the relative concentrations of NOx and VOCs, which dictate the rate of ozone production [52–56]. This study endeavors to leverage satellite remote sensing data to investigate ozone pollution characteristics in Tianjin spanning 2013 to 2022. It aims to delineate primary ozone pollution sources in Tianjin and provide targeted recommendations for mitigating ozone levels based on these findings.

Tianjin, the largest coastal industrial city in northern China, has experienced significant ozone pollution issues in recent years. This city, known for its high population density and its status as the largest port in northern China with a robust petrochemical industry, has faced severe ozone pollution. Despite its critical role, long-term, high-resolution studies on ozone pollution characteristics specific to Tianjin have been lacking. Typically, research on ozone pollution in this region has been integrated into broader studies of the Beijing–Tianjin–Hebei (BTH) metropolitan area.

This paper has addressed the gap by conducting an in-depth analysis of ozone pollution characteristics in Tianjin from 2013 to 2022. Furthermore, a novel method for identifying high-precursor-value zones, based on ozone sensitivity, has been developed. This approach aims to provide more effective local-scale management strategies for ozone pollution.

2. Materials and Methods

2.1. Study Area

Tianjin, a prominent direct-controlled municipality in China, is situated in the northern part of the North China Plain. It is located downstream of the Haihe River, near the Bohai Sea, and is bordered by the Yanshan Mountains to the north. The city's elevation varies from 3.5 to 1052 m above sea level, with geographic coordinates spanning from 116°43′ to 118°04′ east longitude and 38°34′ to 40°15′ north latitude. Tianjin experiences a semi-humid monsoon climate, with an annual average temperature ranging from 11 to 20 °C [57,58]. The city shows distinct monsoonal influences, with peak wind speeds during spring and winter, and lower speeds during summer and autumn, averaging 2 to 4 m per second annually, predominantly from the southwest. According to the "2022 Annual Plan for State-Owned Construction Land Supply" by the Tianjin Municipal Planning and Natural Resources Bureau, the city's total construction land area has reached 4710 hectares, reflecting an 18% increase from 2021. This allocation includes 760 hectares for residential purposes, 150 hectares for commercial and service sectors, 1100 hectares for industrial use, and 2700 hectares for infrastructure and public utilities. The locations indicated in Figure 1 represent 14 ground monitoring stations provided by the Tianjin Environmental Monitoring Center (Figure 1).

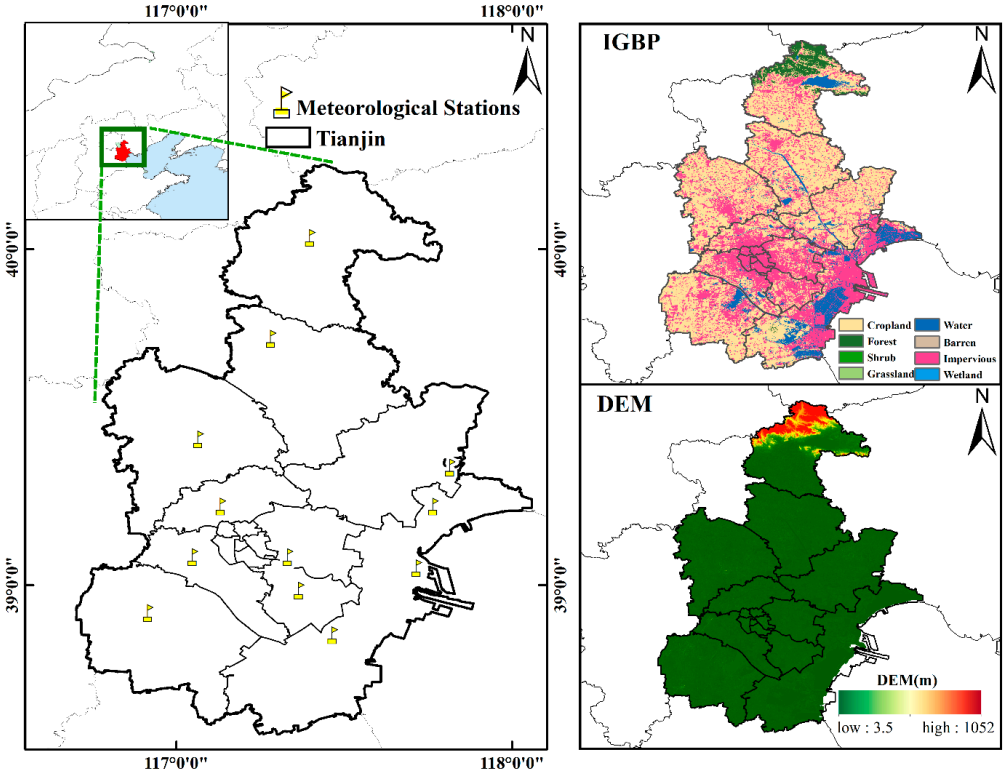


Figure 1. Overview of the study area. IGBP is the land use data of Tianjin, which is mainly classified into eight categories.DEM data range from 3.5−1052m.

2.2. Data Source

2.2.1. Ozone and Its Precursors

This study utilized the Chinese High-resolution and High-quality ground-level Air Pollutant dataset (CHAP), which has provided a comprehensive, long-term, high-resolution record of ground-level air pollutant measurements across China. CHAP has integrated spatial and temporal variability of air pollution using big data derived from artificial intelligence, including ground measurements, remote sensing products, and atmospheric reanalysis data to model pollutants such as $PM_{2.5}$, NO_2, and ozone. In simulating ground-level ozone pollution, The current researchers have introduced an innovative approach

utilizing spatio-temporal extreme random tree models within ensemble learning frameworks. Their methodology has integrated ground observations, remote sensing products, and atmospheric reanalysis data, with a focus on solar radiation intensity and surface temperature, to estimate ground-level ozone concentrations. This approach has produced a high-quality dataset with complete spatial coverage (100%) and fine spatial resolution (1 km), free from cloud interference, missing values, and outliers, and has surpassed many existing satellite products in spatial resolution [3]. This study utilized ground-level ozone concentration data for Tianjin from 2018 to 2022, sourced from the CHAP dataset available at https://zenodo.org/records/13342827, accessed on 20 August 2024. The data have been georeferenced in the GCS_WGS_1984 coordinate system, offering national-level ozone measurements at a spatial resolution of 1 km × 1 km. Prior to analysis, data processing procedures, including cropping and handling of missing values, were performed to extract a dataset specific to ground-level ozone concentrations in Tianjin.

This study utilized data on HCHO and NO_2 column concentrations from the European Space Agency's Sentinel-5 Precursor (Sentinel-5P) TROPOMI mission. Specifically, daily level-2 products for NO_2 (S5P_L2_NO_2) and HCHO (S5P_L2_HCHO) were accessed through ESA's Copernicus Open Access Hub (https://browser.dataspace.copernicus.eu/, accessed on 22 August 2024) [59]. TROPOMI has provided the world's highest spatial resolution in atmospheric remote sensing, with an imaging swath width of 2600 km and a spatial resolution of 5 km × 3.5 km [60]. This resolution improved from 7 km × 3.5 km to 5 km × 3.5 km after 7 August 2019 (http://www.tropomi.eu/mission-status, accessed on 23 August 2024). To ensure uniform spatial resolution and minimize errors, this study employed the Resample tool in ArcGIS 10.8 using the Nearest Neighbor method to standardize HCHO and NO_2 column concentration data to a pixel size of 1 km × 1 km. A satellite-based DOAS algorithm was used for the inversion of tropospheric NO_2 and HCHO vertical column concentrations.

2.2.2. Meteorological Data

This study utilized meteorological data provided by the Global Data Assimilation System (GDAS). GDAS, operated by the National Centers for Environmental Prediction (NCEP), offers high-resolution meteorological observations on a global scale. The dataset includes key meteorological variables such as temperature, humidity, wind speed, and wind direction, spanning multiple atmospheric levels from the surface to the upper atmosphere. These data are generated through advanced numerical weather prediction models and data assimilation techniques, ensuring high timeliness and spatial resolution. The use of GDAS data provided accurate meteorological background information for this study, aiding in the in-depth analysis of the meteorological drivers of ozone pollution in Tianjin.

2.2.3. Other Data

In this study, land use classification data were sourced from the Moderate Resolution Imaging Spectroradiometer (MODIS) Level-3 Land Cover Type product (MCD12Q1). These data were accessed via the MODAPS EOSDIS data archive (https://ladsweb.modaps.eosdis.nasa.gov/search/, accessed on 18 August 2024). Each MODIS product file contained 16 datasets, with this study focusing specifically on the International Geosphere-Biosphere Programme (IGBP) dataset [61]. Urban construction land data for Tianjin were extracted from the MCD12Q1 product utilizing MODIS data processing tools, including the MODIS Reprojection Tool (MRT) and ArcGIS 10.8. A series of operations, including mosaic creation, clipping, geographic coordinate transformation, and class extraction, were performed on the MCD12Q1 land cover type data to generate the Tianjin land cover dataset based on the IGBP classification.

2.3. Method

2.3.1. Automated High-Value Area Identification Technology

Initially, this study integrated data on ozone and its precursor concentrations. Tianjin was spatially partitioned into numerous primary remote sensing units based on established geographical divisions, each centered at specific coordinates to provide unit location data. This segmentation resulted in 14,032 first-level remote sensing units, each covering 1×1 km^2.

Subsequently, secondary remote sensing units were delineated by overlaying land use classifications, urban built-up area data, and enterprise listings. Satellite remote sensing technology was employed to derive concentration data for HCHO and NO_2 columns, with the HCHO/NO_2 ratio serving as an indicator for ozone precursor levels. By combining this ratio with Tianjin's ozone sensitivity threshold, areas sensitive to ozone generation were identified.

For regions subject to VOC control or dual control involving VOCs and NOx, HCHO column concentration data were utilized to reduce natural source interference, identifying VOC-dominated areas primarily influenced by industrial emissions. As a tertiary remote sensing unit, high-value VOC areas were pinpointed as focal points by cross-referencing with high-resolution satellite images (Figure 2).

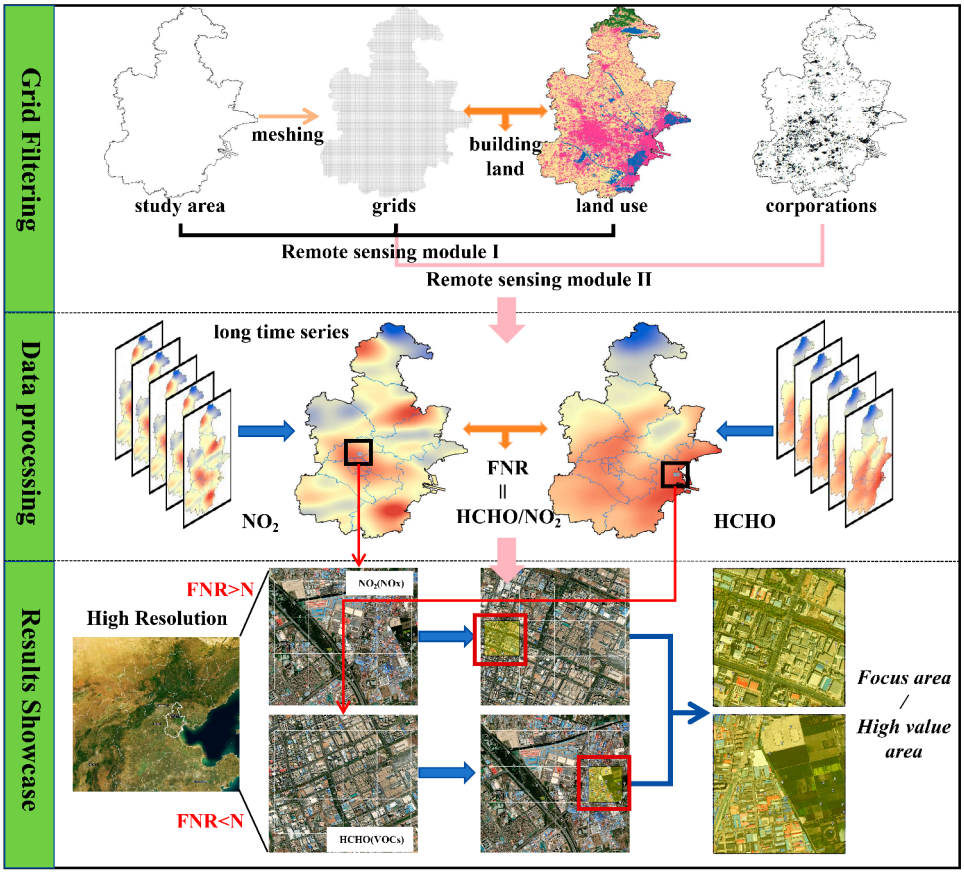


Figure 2. Methodological process for identifying high−value areas for ozone precursors. The NO_2 and HCHO stretching values during the data processing stage ranged from 0−1200 and 0−3400 molecules/cm^2, respectively.

This structured approach facilitated a comprehensive analysis of ozone pollution characteristics and sources in Tianjin, providing insights into key areas requiring targeted mitigation strategies.

2.3.2. Minimum Least Squares (MLS)

Minimum Least Squares (MLS) is a widely adopted statistical technique in data analysis and regression modeling. It serves as a fundamental method for determining the best-fitting line or curve to a set of observed data points by minimizing the sum of squared residuals, which are the squared differences between observed values and those predicted by the model. MLS is particularly effective in linear regression, where it estimates the parameters of a linear function that best describes the relationship between dependent and independent variables. The resulting linear model provides insights into the nature of a relationship and enables predictions for new data points.

2.3.3. Backward Trajectory Clustering Analysis

This study utilized Meteoinfo3.9.6 software, integrating the Hybrid Single-Particle Lagrangian Integrated Trajectory (HYSPLIT) model and Global Data Assimilation System (GDAS) data from NCEP. The software simulated backward trajectories to assess the influence of air masses over Tianjin. These trajectories underwent Eulerian distance clustering analysis based on movement speed and transport direction, resulting in distinct categories of transport paths. The analysis, conducted in Tianjin, examined hourly backward trajectories of air masses from June each year between 2018 and 2022. Trajectories were computed daily, starting at 00:00 UTC, and simulated in reverse for 24 h at an altitude of 500 m. This methodology aimed to elucidate spatial patterns and temporal dynamics in the transport of air masses.

3. Results

3.1. Spatio-Temporal Variations of Ground-Level Ozone in Tianjin Between 2013 and 2022

3.1.1. Spatio-Temporal Characteristics

In our detailed analysis of daily ozone data from Tianjin spanning 2013 to 2022, we have employed probabilistic density statistical methods to characterize the annual distribution of ozone concentrations. Specifically, the Poisson distribution model has been utilized to approximate the probability distribution of these discrete data.

Our comparative analysis of the Poisson distribution curves for each year has revealed a significant rightward shift from 2013 to 2022. This shift has indicated that the distribution of ozone concentrations has progressively moved from levels below 100 $\mu g/m^3$ (the reference standard in this study) to levels exceeding this standard. This trend reflects an overall increase in ozone concentrations in Tianjin.

A comparison of the mean ozone concentrations for the periods 2013–2017 and 2018–2022 shows the following: On the one hand, the peak of the fitted curve has undergone a significant backward shift, indicating a significant increase in both the peak and mean; on the other hand, the mean of the number of days with high values has increased significantly. In the 160–240 $\mu g/m^3$ interval, it increases from an average of 18 days per year in 2013–2017 to 65 days in 2018–2022. According to the Technical Regulations on Ambient Air Quality Index (HJ 633–2012), ozone-polluted days have been defined as those with a daily MDA8 ozone concentration exceeding 160 $\mu g/m^3$. Ozone pollution levels have been categorized into mild (160–215 $\mu g/m^3$), moderate (216–265 $\mu g/m^3$), and heavy (>266 $\mu g/m^3$). From 2013 to 2022, the number of days with ozone pollution in Tianjin has increased from 20 days (all of which were classified as mild pollution, 6.431%) to 74 days (17.66%), comprising 61 days (14.558%) of mild pollution, 11 days (2.625%) of moderate pollution, and 2 days (0.477%) of severe pollution. Throughout this period, the number of polluted days has exhibited a fluctuating upward trend (Figure 3).

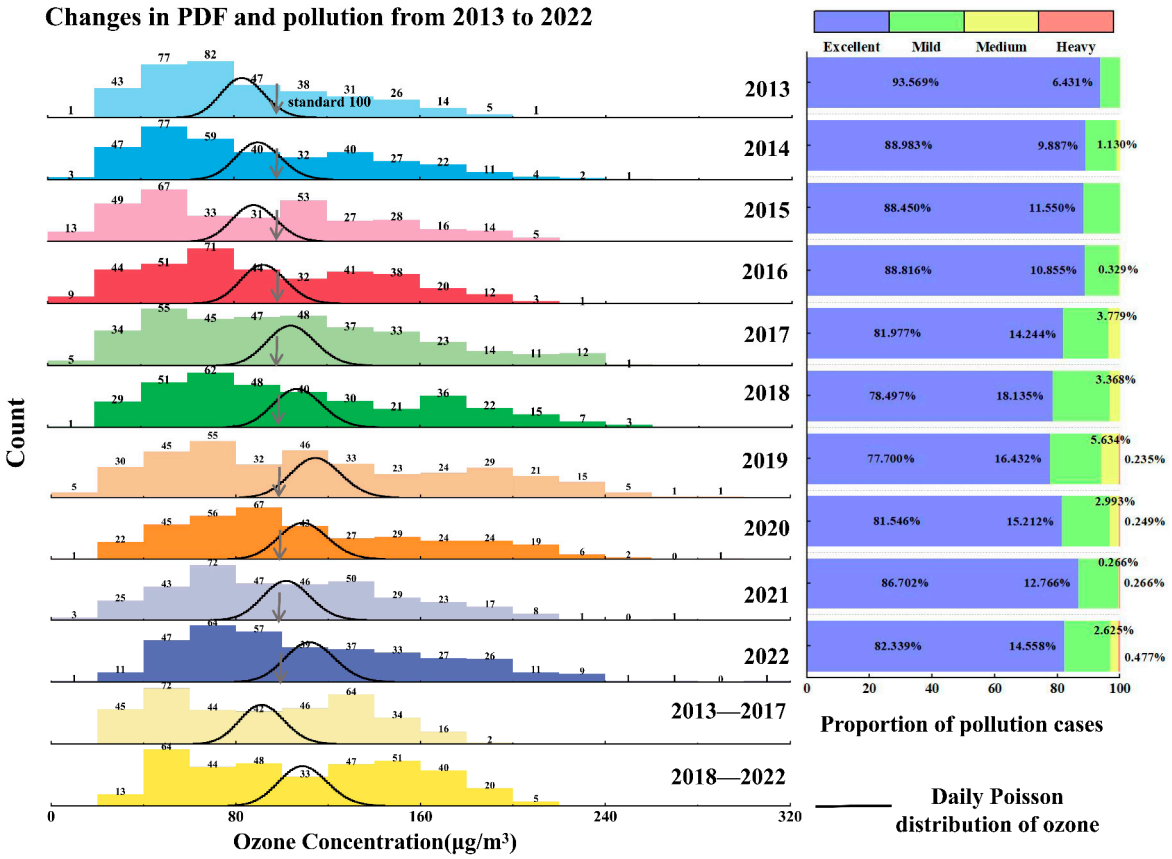


Figure 3. Changes in PDF and pollution from 2013 to 2022.Excellent (<160 μg/m^3), Mild (160−215 μg/m^3), Medium (216−265 μg/m^3), Heavy (>265 μg/m^3).

As one of China's four direct-controlled municipalities, Tianjin has experienced an average ozone concentration ranging from 91 to 105 μg/m^3 over this period. In several areas of Tianjin, including northeastern Ninghe District, southern Jinghai District, and southern Binhai New Area, the ozone concentration has exceeded the Class I standard of the "Ambient Air Quality Standards" (GB 3095–2012) [62], which is 100 μg/m^3. In Tianjin, the average concentration distribution of ozone from 2013 to 2022 exhibits a pronounced gradient, with higher levels in the south and lower levels in the north. The areas of highest concentration are primarily located in Jinghai and the southern part of Binhai, where the average concentration reached 100.6081 μg/m^3, ranking fifth nationally (Figure S1a,b). Additionally, the growth rate of ozone concentrations is notably higher in the central urban areas compared to the surrounding districts. The highest growth values are concentrated in the regions of Wuqing, Beichen, and Hedong, with an average growth rate of 34.09%, also placing it fifth in the national rankings (Figure S1c,d).

From 2013 to 2022, ground-level ozone concentrations in Tianjin have demonstrated a fluctuating upward trend, with the highest daily average recorded in 2019 at 114.88 μg/m^3. By 2022, the peak daily ozone concentration had reached 305.50 μg/m^3, with an average annual growth rate of 2.84 μg·m^3·yr^{-1}. As shown by the curves in Figure S1e, the pollution peaks and average values in Tianjin were significantly higher than those in the three major urban agglomerations. Among the three major urban agglomerations, the ozone fluctuation was the largest in the Beijing–Tianjin–Hebei region, and the fluctuation was the smallest in the Pearl River Delta region. In terms of growth rate, Tianjin > YRD > BTH > national average > PRD.

High ozone pollution levels in different geographical areas are influenced by various factors. In the YRD region, increased solar radiation, rising temperatures, and declining sea levels contribute to ozone pollution. In the BTH region, elevated ozone concentrations

are primarily attributed to precursor emissions. These diverse factors collectively lead to varying levels of ozone pollution across different regions.

3.1.2. Seasonal Distribution Characteristics

The period from 2013 to 2022 has been categorized into four seasons: spring (March to May), summer (June to August), autumn (September to November), and winter (December to February). Given Tianjin's relatively small area, optimal stretching values for each season have been determined. The results indicate that the stretching ranges for ozone concentrations are as follows: 100–120 μg/m^3 in spring, 120–160 μg/m^3 in summer, 70–90 μg/m^3 in autumn, and 45–65 μg/m^3 in winter. Seasonal ground-level ozone concentrations in Tianjin have been ranked as follows: summer > spring > autumn > winter. Specifically, high ozone values in spring have been concentrated in northeastern Ninghe, southern Jinghai, and southern Binhai (Figure 4a). In summer, elevated values have been observed predominantly in Wuqing, Jinghai, and Binhai (Figure 4b). During autumn, high concentrations have been most pronounced in southeastern Jinghai District and southern Binhai New Area (Figure 4c). In winter, elevated values have been concentrated in northern Jizhou District (Figure 4d).

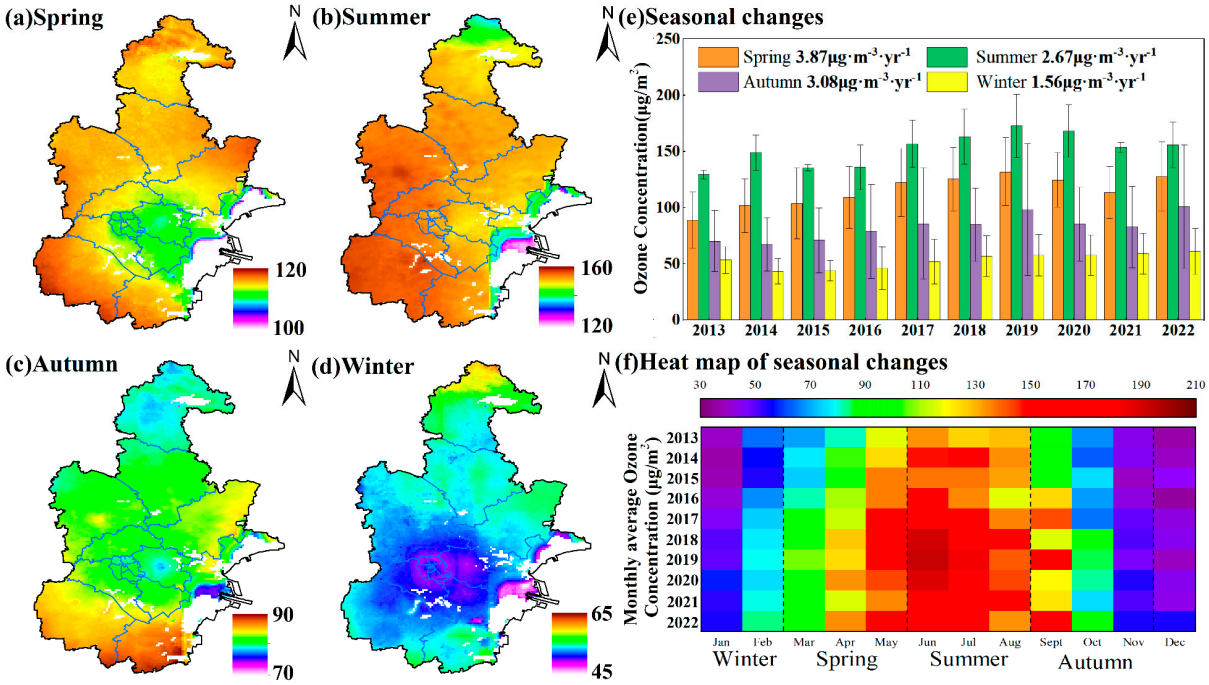


Figure 4. Seasonal changes in ground−level ozone, 2013−2022. The (**a**–**d**) represent the average concentration distributions for the four seasons spanning from 2013 to 2022, while (**e**) depicts the concentration variations and variation rates across the four seasons over the same period (2013−2022). Additionally, (**f**) presents a heatmap of the concentration changes.

From 2013 to 2022, all seasons have exhibited varying degrees of increases in ozone concentrations, with average annual growth rates of 3.87 μg/m^3 in spring, 2.67 μg/m^3 in summer, 3.08 μg/m^3 in autumn, and 1.56 μg/m^3 in winter (Figure 4e). An analysis of the monthly average concentration heatmaps (Figure 4f) has indicated that from February to March 2022, the increase in spring and autumn was significantly higher compared to summer. This suggests that, despite ongoing pollution during summer, ozone pollution has gradually expanded into spring and autumn.

3.2. Analysis of Ground-Level Ozone Pollution Conditions

We have analyzed the potential causes of six moderate to severe ground-level ozone pollution events (HOEs) in Tianjin from May to September 2022 (Table 1). Typical pollution

events have been defined as those with average concentrations exceeding 170 μg/m^3, peak concentrations surpassing 200 μg/m^3, and a cumulative duration exceeding five days. HOE4 persisted for 13 days, followed by HOE3 and HOE5, each lasting 10 days, with HOE6 being the shortest at 6 days. During HOE3, ground-level ozone concentrations increased significantly from 160 μg/m^3 to 305 μg/m^3 between 24 and 25 June. Figure 5 shows the wind field distribution and backward trajectory source analysis during six pollution events.

Table 1. Six heavy ozone pollution episodes (HOEs) in Tianjin in 2022.

Event	Date	Duration (Days)	Mean Ozone Concentrations (μg·m^{-3})	Maximum Daily Ozone Concentration (μg·m^{-3})
HOE1	17 May–24 May 2022	8	205.5677	224.6471
HOE2	28 May–3 June 2022	7	201.8549	275.6492
HOE3	16 June–25 June 2022	10	206.9922	305.4954
HOE4	13 July–25 July 2022	13	176.7147	202.0923
HOE5	8 September–17 September 2022	10	186.6930	229.8277
HOE6	25 September–30 September 2022	6	205.3579	230.8500

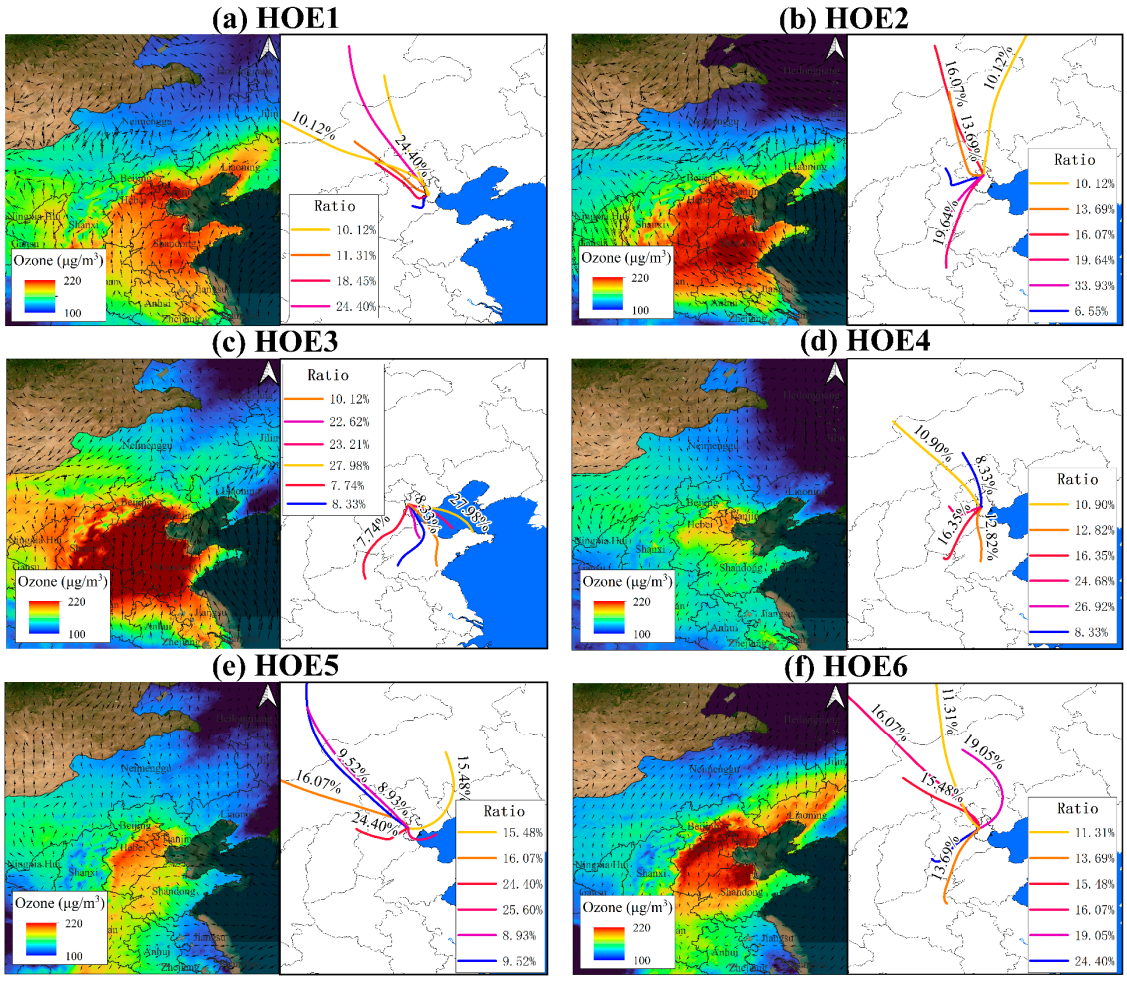


Figure 5. (**a**–**f**) Six pollution events, each of which is divided into two graphs. The left graph is based on the average concentration during the pollution period, overlaid with the wind field during the pollution period. The right graph shows the 7-day backward trajectory of the peak pollution point during the pollution period.

In addition to local accumulation, ozone pollution is influenced by regional and inter-terrain transport. To investigate this, we conducted backward trajectory analyses for seven days prior to each pollution event at an altitude of 500 m. The results revealed that during HOE1, the peak pollution was observed in Wuqing District, with air masses predominantly originating from the west, particularly from Beijing and Hebei. It is noteworthy that the contribution from the route through Beijing has amounted to 64.28%, with contributions from northern and western Shandong (Figure 5a).

During HOE2, the heaviest pollution occurred in Baodi District, with significant air mass transport from the southwest of Tianjin. Transport through Langfang in Hebei and western Shandong contributed 53.57% of the pollution (Figure 5b). In HOE3, the peak pollution was centered in central Wuqing District, with air masses predominantly from the southeast and notable monsoon influences. High ozone concentrations were also recorded in other eastern Chinese cities, attributed to a sharp rise in temperature in June that intensified local photochemical reactions. The severe pollution event was driven by a combination of local generation and 7.74% transport from the southwest (Figure 5c).

HOE4′s pollution was concentrated in Beichen District, with reduced severity compared to HOE3. The primary air masses originated from western Hebei, including Langfang and Baoding, contributing 24.68% of the pollution (Figure 5d). During HOE5, the pollution center was in western Wuqing District, with significant transport from Baoding in Hebei contributing 24.4%. Additionally, southeastern transport accounted for 25.6%, and transport from Zhangjiakou and Inner Mongolia via Beijing contributed 34.52% (Figure 5e). For HOE6, high concentrations were observed along the Beijing–Baoding-Shijiazhuang corridor, with transport from high-value areas contributing 24.4%. Transport from northern Zhangjiakou via Beijing accounted for 42.86% (Figure 5f).

3.3. Effects of Precursors on Ground-Level Ozone

This study has investigated the influence of local photochemical reactions on ground-level ozone concentrations in Tianjin from 2018 to 2022. It has aimed to identify critical sources of ozone precursors and periods of increased sensitivity to ozone generation. Initially, this study identified periods of heightened sensitivity to ozone formation during pollution events in Tianjin. Subsequently, it analyzed representative species of major ozone precursors and their correlation with ground-level ozone concentrations. This analysis has determined which precursor species should be prioritized for effective mitigation of ground-level ozone formation during pollution events. Finally, this study utilized enterprise information to identify areas with elevated precursor concentrations. This approach has sought to manage ozone formation indirectly by targeting regions with high values of ozone precursors.

3.3.1. Ozone Generation Sensitivity Analysis

Ozone generation in urban environments like Tianjin has been significantly influenced by VOCs and NOx, which serve as essential precursors in the photochemical process. The relationship governing ozone formation is nonlinear and contingent upon the concentrations of these precursors. Therefore, understanding the sensitivity of ozone formation to VOCs and NOx is crucial. Ren et al. have investigated sensitivity thresholds for ozone formation in the Beijing–Tianjin–Hebei (BTH) region from 2013 to 2021. They have found that the Fraction of NOx Remaining (FNR), which indicates the control mechanism of ozone formation, ranged from 3.0 to 3.8. When the FNR is below 3.0, ozone formation is primarily controlled by VOCs; when between 3.0 and 3.8, it is controlled by both VOCs and NOx; and when above 3.8, it is predominantly controlled by Nox [57]. In the recent study conducted by Zheng et al., peak fitting analysis based on HCHO and NO_2 column concentrations has indicated a peak Fraction of NOx Remaining (FNR) value of 3.06, with a transition range between 2.67 and 3.47. Areas with FNR values below 2.67 have been classified as VOC-limited, those between 2.67 and 3.47 as transition zones, and those above 3.47 as NOx-limited [63].

In this study, the FNR threshold range has been established between 2.67 and 3.47. Areas with an FNR below 2.67 have been classified as VOC control zones, while those within the range of 2.67 to 3.47 have been categorized as VOC-NOx co-control zones. An FNR exceeding 3.47 has designated a NOx control zone. Using column concentrations of HCHO and NO_2 for the year 2022, this study has mapped the sensitivity of ozone generation in Tianjin. The findings have demonstrated that in 2022, ozone formation in Tianjin has been primarily regulated by VOCs or through synergistic VOC-NOx control (Figure 6a). Sensitivity distributions for ozone generation have been derived by calculating the FNR ($HCHO/NO_2$) for the entire year as well as for June 2022. This methodology has provided a comprehensive framework for understanding and managing ozone pollution in Tianjin, which is essential for the development of effective environmental policies and pollution control strategies in urban areas.

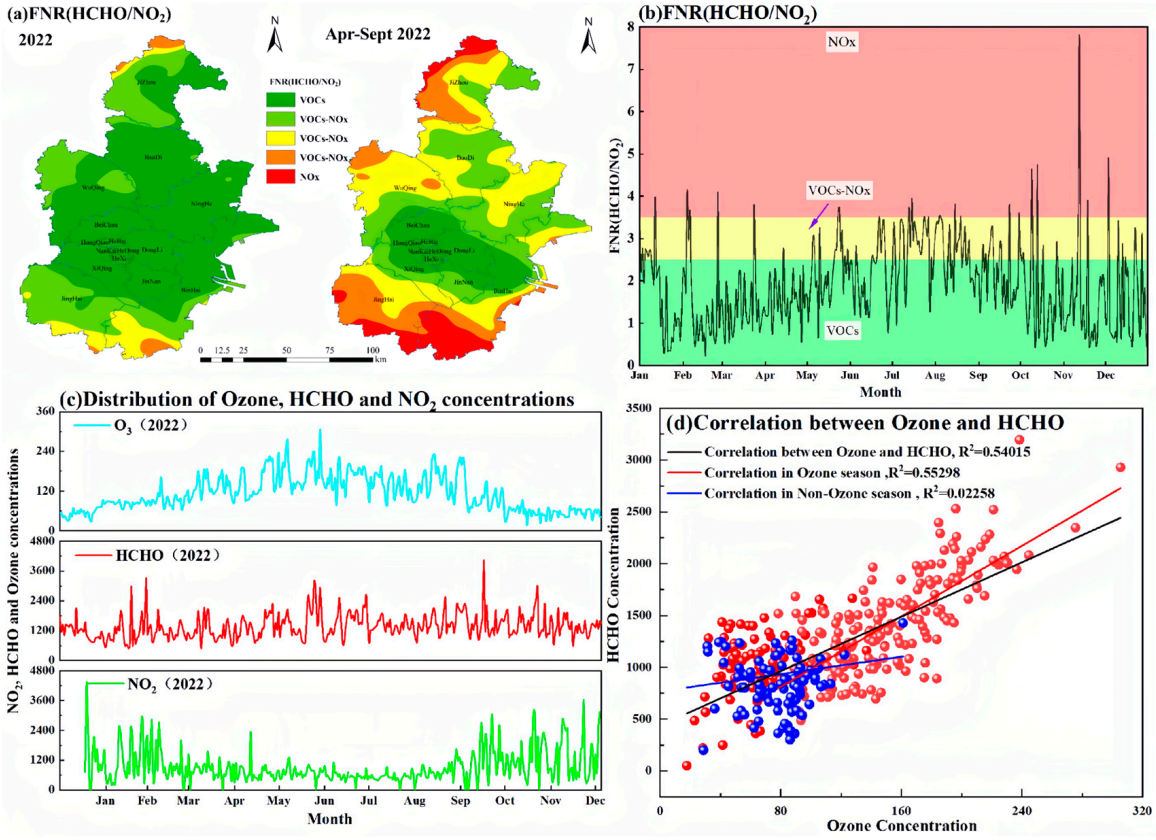


Figure 6. (**a**) Distribution of FNR (**b**) Time variation of FNR. (**c**) Distribution of ground−level ozone, HCHO, and NO_2, concentrations in 2022. (**d**) Correlation between ozone and HCHO, Red dots represent HCHO and ozone concentrations during the ozone season and blue dots represent the non-ozone season.

For this study, we have analyzed daily ground-level ozone concentrations alongside HCHO and NO_2 column densities in Tianjin for the year 2022. In 2022, the average ground-level ozone concentration in Tianjin was 112.328 μg/m^3, with HCHO column density averaging 1396 × 10^{13} molecules/cm^2 and NO_2 column density averaging 1122 × 10^{13} molecules/cm^2 (Figure 6b). Our analysis of NO_2 and HCHO column densities for 2022 has revealed that ozone formation in Tianjin is primarily influenced by VOCs and the interactive effects of NOx and VOCs (Figure 6c). HCHO, as a key intermediate in photochemical reactions, has served as an indicator for VOC distribution. The correlation between HCHO and ground-level ozone in Tianjin in 2022 has been notably strong, with an R^2 value of 0.54015 ($p < 0.01$). During the ozone season (April to September), this correlation was slightly higher, with an R^2 value of 0.55298 ($p < 0.01$). In contrast, during

the non-ozone season (January to March and October to December), the correlation was substantially lower, with an R^2 value of 0.02258 ($p < 0.01$) (Figure 6d).

3.3.2. Results of High-Value Areas of HCHO

In response to the aforementioned findings, we have developed a system aimed at swiftly identifying regions with elevated concentrations of ozone and its precursors during pollution events. This system, implemented using Python3.8, integrates relevant APIs for spatial automation and high-value area identification. It furnishes comprehensive data to support on-site investigations of pollutant emissions from industrial sources. Key inputs include NO_2 and HCHO column densities alongside ground-level ozone concentrations. By classifying controlled area types within ozone-affected regions, targeted strategies for ozone pollution mitigation can be effectively deployed. For this system, we illustrate our identification process using selected high-value areas identified in June 2022.

This study proceeds through five main stages. Initially, data pre-processing involves preparing processed NO_2 (Figure 7a), HCHO (Figure 7b) column concentrations, and ground-level ozone data with consistent spatial and temporal resolutions. Spatial uniformity is achieved using the Cubic Spline resampling method, with a uniform spatial resolution of $0.01^\circ \times 0.01^\circ$. Subsequently, ozone sensitivity analysis is conducted for Tianjin, illustrated in Figure 7c for June 2022. The analysis reveals predominant VOC and VOC-NOx control in most areas of Tianjin, with NOx influence evident in southern and northern regions. Integration of subsurface enterprise data (Figure 7d) and land use classification, combined with defined screening thresholds, identifies HCHO concentration hotspots in Tianjin for June 2022. Figure 7e highlights eight high-value zones across four districts and counties: one in Wuqing District, two each in Xiqing, Jinghai, Jinnan Districts, and Binhai New District. These zones intersect with several enterprises, marked with white indicators in the figure, signifying areas requiring focused attention.

Utilizing this approach, we have performed a monthly identification of high-HCHO-value areas in Tianjin for the year 2022. In total, we have identified 114 high-value grids (1×1 km^2), with the majority located in Binhai New Area (23 grids, including 1 duplicate) and Wuqing District (21 grids, including 4 duplicates). All districts, with the exception of Nankai District, have exhibited varying numbers of identified high-value grids (Figure 8a).

The monthly analysis has shown that June exhibited the highest number of identified high-value grids, followed by September and October. The distribution of HCHO and ground-level ozone concentrations has revealed a strong correlation between June and September (Figure 8b). Further comparison between ozone season and non-ozone season data has indicated that the correlation between HCHO and ground-level ozone across all identified high-value grids is $R^2 = 0.27546$. During the ozone season, this correlation improves to $R^2 = 0.56339$, whereas in the non-ozone season, it is $R^2 = 0.2241$. These enhanced correlations, compared to those illustrated in Figure 8c, underscore the effectiveness of high-value area identification for ozone precursors in the targeted management of ozone pollution.

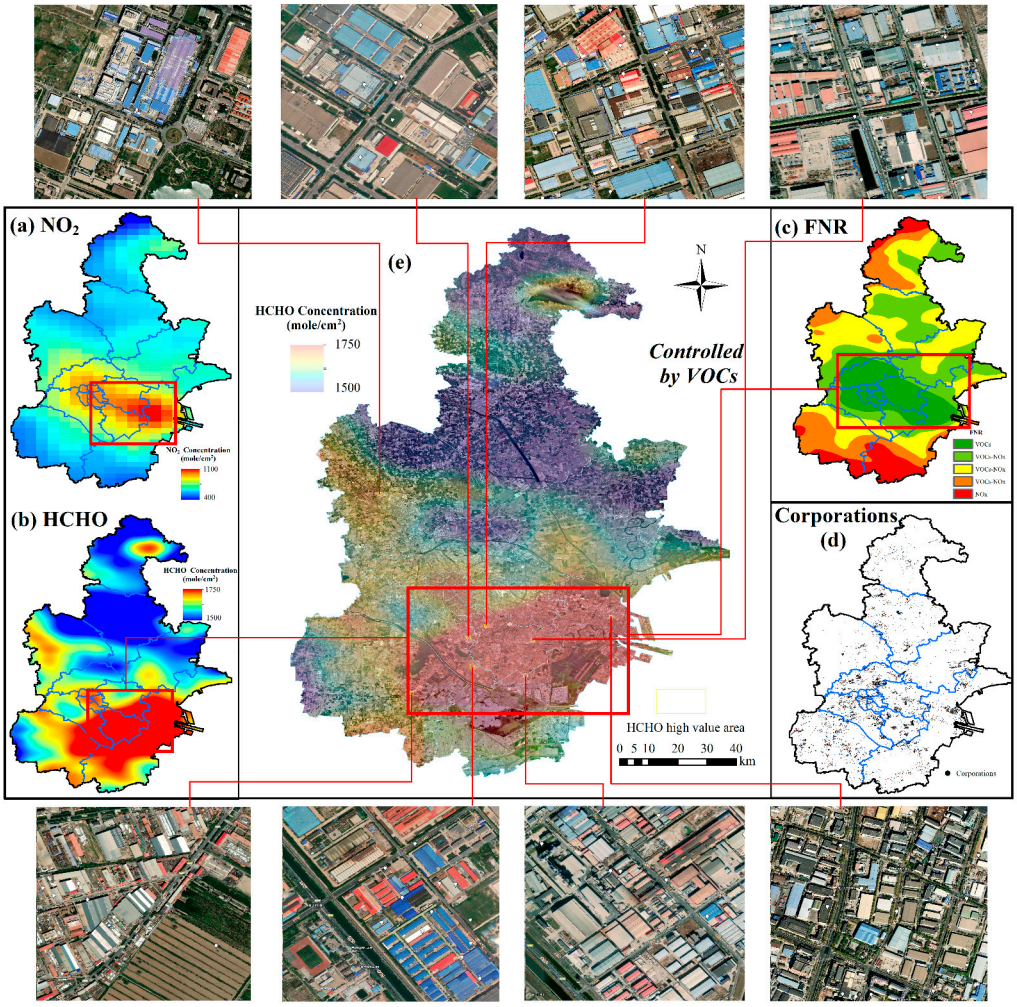


Figure 7. Technical process for identifying high−value areas for ozone precursors and identification results; (**a**) NO_2 column concentration distribution; (**b**) HCHO column concentration distribution; (**c**) ozone generation sensitivity index (FNR); (**d**) Tianjin Enterprise Points; (**e**) high-value area screening results.

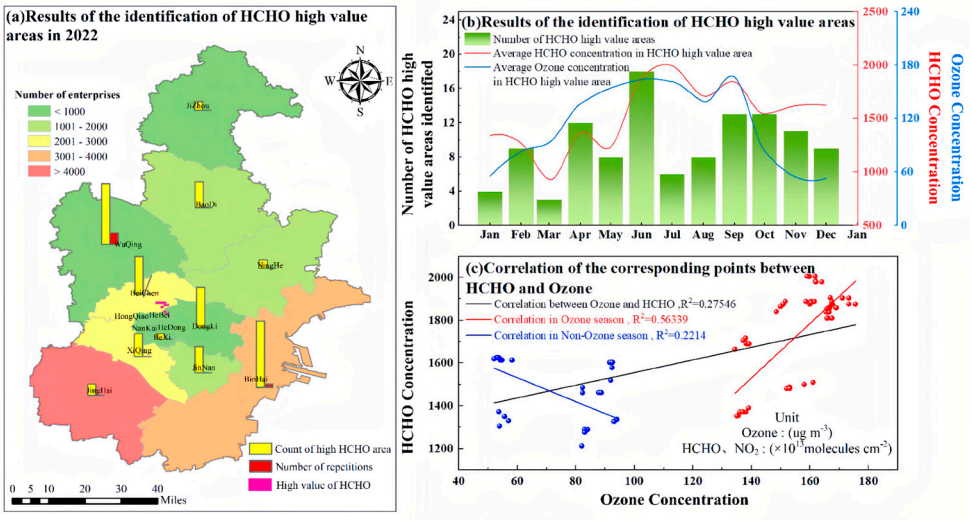


Figure 8. (**a**) Results of the identification of high−HCHO−value areas in 2022. (**b**) Results of the identification of high−HCHO−value areas. (**c**) Correlation of the corresponding points between HCHO and ozone.

4. Discussion

In this study, we analyze the characteristics and sources of ozone pollution in Tianjin from 2013 to 2022. By integrating ground-level ozone concentrations from the CHAP dataset with satellite observations of HCHO and NO_2 from TROPOMI, we employed back trajectory modeling and high-value area identification methods for ozone precursors to investigate the direct and indirect factors influencing ozone formation. Our findings indicate that air masses originating from the northwest and southwest significantly affect ozone levels in Tianjin. Additionally, the high-value area identification results provide robust data support for ozone management strategies. However, this study has certain limitations. First, the inversion process for HCHO and NO_2 observational data may introduce errors that could affect the final identification results. Furthermore, the lack of long-term data on near-surface ozone and its precursors restricts the assessment of their long-term trends. Future research should enhance the accuracy of original data processing, thereby providing stronger data support for ozone pollution management in the Beijing–Tianjin–Hebei region and nationwide. We also identify substantial potential for improvement in the high-value area identification methods for ozone precursors. Enhancements at the foundational level should focus on increasing the accuracy of data sources, while the second level pertains to the various factors influencing the FNR values based on TROPOMI data. Future studies could benefit from improved temporal and spatial resolution to facilitate more detailed analyses. Finally, integrating emission data from industrial sources in future research will allow for more precise identification of pollutant-emitting enterprises or zones, thus enhancing the targeted nature of the identification results. We aim to continue our investigations to achieve a more precise understanding of the causes of ozone pollution.

5. Conclusions

From 2013 to 2022, Tianjin ranked fifth nationwide in both average ground-level ozone concentration and average annual growth rate. The average concentration was 100.61 $\mu g/m^3$, with an average growth rate of 34.09%. The number of polluted days increased from 20 days in 2013 (all mild pollution) to 74 days in 2022 (including 61 days of mild pollution, 11 days of moderate pollution, and 2 days of severe pollution). Comparatively, Tianjin's average annual growth rate of 2.84 $\mu g/m^3$ was the highest among major urban regions, with pollution levels exceeding those in other city clusters. Seasonal variations in ground-level ozone concentrations in Tianjin showed the highest concentrations in summer, followed by spring, autumn, and winter. The average growth rate was highest in spring, followed by autumn, summer, and winter, indicating a trend of ozone pollution extending into spring and autumn.

An analysis of six pollution events in 2022 revealed that Tianjin's ozone pollution is significantly influenced by regional transport, primarily from industrial emissions in southern Hebei and northern Shandong. Therefore, effective control measures should balance and coordinate strategies for managing various air pollutants, consider the critical role of meteorological conditions, and enhance regional cooperation in air quality management.

Tianjin's ozone pollution is primarily controlled by VOCs or the synergistic effect of VOCs and NOx. The identification of high-value areas for ozone precursors, using HCHO as a representative for VOCs, is significant for ozone management. During both ozone and non-ozone seasons, the correlation between HCHO and ozone is higher in identified high-value grids compared to non-high-value areas.

Supplementary Materials: The following supporting information can be downloaded at: https://www.mdpi.com/article/10.3390/rs16213970/s1, Figure S1 is shown in the Supplementary File.

Author Contributions: Conceptualization, W.Z. and X.Y.; formal analysis and writing—original draft preparation, S.D.; data curation, L.C. and L.W.; writing—review and editing, P.M. and N.L.; methodology, all co-authors. All authors have read and agreed to the published version of the manuscript.

Funding: This research was supported by Beijing Natural Science Foundation (Grants 8242023) and National Key Research and Development Programme of China (Grant 2022YFC3700104).

Data Availability Statement: The original contributions presented in the study are included in the article/Supplementary Materials, further inquiries can be directed to the corresponding author.

Conflicts of Interest: The funders had no role in the design of this study; in the collection, analyses, or interpretation of data; in the writing of the manuscript; or in the decision to publish the results.

References

1. Liu, J.; Wang, S.; Yuan, Q.; Zhang, F.; Zhu, L. Vertical Profile of Ozone Derived from Combined MLS and TES Satellite Observations. *Remote Sens.* **2022**, *14*, 1588. [CrossRef]
2. Liu, J.; Strode, S.A.; Liang, Q.; Oman, L.D.; Colarco, P.R.; Fleming, E.L.; Manyin, M.E.; Douglass, A.R.; Ziemke, J.R.; Lamsal, L.N.; et al. Change in Tropospheric Ozone in the Recent Decades and Its Contribution to Global Total Ozone. *JGR Atmos.* **2022**, *127*, e2022JD037170. [CrossRef]
3. Wei, J.; Li, Z.; Li, K.; Dickerson, R.R.; Pinker, R.T.; Wang, J.; Liu, X.; Sun, L.; Xue, W.; Cribb, M. Full-Coverage Mapping and Spatiotemporal Variations of Ground-Level Ozone (O3) Pollution from 2013 to 2020 across China. *Remote Sens. Environ.* **2022**, *270*, 112775. [CrossRef]
4. Zou, M.; Xiong, X.; Wu, Z.; Yu, C. Ozone Trends during 1979–2019 over Tibetan Plateau Derived from Satellite Observations. *Front. Earth Sci.* **2020**, *8*, 579624. [CrossRef]
5. Wang, Y.; Hopke, P.K.; Xia, X.; Rattigan, O.V.; Chalupa, D.C.; Utell, M.J. Source Apportionment of Airborne Particulate Matter Using Inorganic and Organic Species as Tracers. *Atmos. Environ.* **2012**, *55*, 525–532. [CrossRef]
6. Lei, R.; Zhu, F.; Cheng, H.; Liu, J.; Shen, C.; Zhang, C.; Xu, Y.; Xiao, C.; Li, X.; Zhang, J.; et al. Short-Term Effect of PM2.5/O3 on Non-Accidental and Respiratory Deaths in Highly Polluted Area of China. *Atmos. Pollut. Res.* **2019**, *10*, 1412–1419. [CrossRef]
7. Liu, H.; Liu, S.; Xue, B.; Lv, Z.; Meng, Z.; Yang, X.; Xue, T.; Yu, Q.; He, K. Ground-Level Ozone Pollution and Its Health Impacts in China. *Atmos. Environ.* **2018**, *173*, 223–230. [CrossRef]
8. Tian, Y.; Wu, Y.; Liu, H.; Si, Y.; Wu, Y.; Wang, X.; Wang, M.; Wu, J.; Chen, L.; Wei, C.; et al. The Impact of Ambient Ozone Pollution on Pneumonia: A Nationwide Time-Series Analysis. *Environ. Int.* **2020**, *136*, 105498. [CrossRef]
9. Yang, P.; Zhang, Y.; Wang, K.; Doraiswamy, P.; Cho, S.-H. Health Impacts and Cost-Benefit Analyses of Surface O3 and PM2.5 over the U.S. under Future Climate and Emission Scenarios. *Environ. Res.* **2019**, *178*, 108687. [CrossRef]
10. Yuan, Y.; Wu, Y.; Ge, X.; Nie, D.; Wang, M.; Zhou, H.; Chen, M. In Vitro Toxicity Evaluation of Heavy Metals in Urban Air Particulate Matter on Human Lung Epithelial Cells. *Sci. Total Environ.* **2019**, *678*, 301–308. [CrossRef]
11. Feng, Z.; Xu, Y.; Kobayashi, K.; Dai, L.; Zhang, T.; Agathokleous, E.; Calatayud, V.; Paoletti, E.; Mukherjee, A.; Agrawal, M.; et al. Ozone Pollution Threatens the Production of Major Staple Crops in East Asia. *Nat. Food* **2022**, *3*, 47–56. [CrossRef] [PubMed]
12. Zhao, S.; Yang, X.; Li, Z.; Wang, Z.; Zhang, Y.; Wang, Y.; Zhou, C.; Ma, P. Sixty years of progress in satellite remote sensing of ozone. *J. Remote Sens.* **2022**, *26*, 817–833.
13. Ding, D.; Xing, J.; Wang, S.; Liu, K.; Hao, J. Estimated Contributions of Emissions Controls, Meteorological Factors, Population Growth, and Changes in Baseline Mortality to Reductions in Ambient PM2.5 and PM2.5-Related Mortality in China, 2013–2017. *Environ. Health Perspect.* **2019**, *127*, 067009. [CrossRef] [PubMed]
14. Cao, T.; Wang, H.; Li, L.; Lu, X.; Liu, Y.; Fan, S. Fast Spreading of Surface Ozone in Both Temporal and Spatial Scale in Pearl River Delta. *J. Environ. Sci.* **2024**, *137*, 540–552. [CrossRef] [PubMed]
15. Lu, X.; Hong, J.; Zhang, L.; Cooper, O.R.; Schultz, M.G.; Xu, X.; Wang, T.; Gao, M.; Zhao, Y.; Zhang, Y. Severe Surface Ozone Pollution in China: A Global Perspective. *Environ. Sci. Technol. Lett.* **2018**, *5*, 487–494. [CrossRef]
16. Lyu, Y.; Wu, H.; Liu, X.; Han, F.; Lv, F.; Pang, X.; Chen, J. Co-Occurring Extremes of Fine Particulate Matter ($PM_{2.5}$) and Ground-Level Ozone in the Summer of Southern China. *Geophys. Res. Lett.* **2024**, *51*, e2023GL106527. [CrossRef]
17. Ma, X.; Huang, J.; Zhao, T.; Liu, C.; Zhao, K.; Xing, J.; Xiao, W. Rapid Increase in Summer Surface Ozone over the North China Plain during 2013–2019: A Side Effect of Particulate Matter Reduction Control? *Atmos. Chem. Phys.* **2021**, *21*, 1–16. [CrossRef]
18. Wang, W.; Parrish, D.D.; Wang, S.; Bao, F.; Ni, R.; Li, X.; Yang, S.; Wang, H.; Cheng, Y.; Su, H. Long-Term Trend of Ozone Pollution in China during 2014–2020: Distinct Seasonal and Spatial Characteristics and Ozone Sensitivity. *Atmos. Chem. Phys.* **2022**, *22*, 8935–8949. [CrossRef]
19. Wu, K.; Wang, Y.; Qiao, Y.; Liu, Y.; Wang, S.; Yang, X.; Wang, H.; Lu, Y.; Zhang, X.; Lei, Y. Drivers of 2013–2020 Ozone Trends in the Sichuan Basin, China: Impacts of Meteorology and Precursor Emission Changes. *Environ. Pollut.* **2022**, *300*, 118914. [CrossRef]
20. Zhang, A.; Lin, J.; Chen, W.; Lin, M.; Lei, C. Spatial–Temporal Distribution Variation of Ground-Level Ozone in China's Pearl River Delta Metropolitan Region. *Int. J. Environ. Res. Public Health* **2021**, *18*, 872. [CrossRef]
21. Zhu, S.; Ma, J.; Wang, S.; Sun, S.; Wang, P.; Zhang, H. Shifts of Formation Regimes and Increases of Atmospheric Oxidation Led to Ozone Increase in North China Plain and Yangtze River Delta From 2016 to 2019. *JGR Atmos.* **2023**, *128*, e2022JD038373. [CrossRef]
22. Wang, Y.; Yuan, Q.; Li, T.; Zhu, L.; Zhang, L. Estimating Daily Full-Coverage near Surface O3, CO, and NO2 Concentrations at a High Spatial Resolution over China Based on S5P-TROPOMI and GEOS-FP. *ISPRS J. Photogramm. Remote Sens.* **2021**, *175*, 311–325. [CrossRef]
23. Chang, F.; Li, J.; Li, N.; Liao, H. Stratospheric Intrusion May Aggravate Widespread Ozone Pollution through Both Vertical and Horizontal Advections in Eastern China during Summer. *Front. Environ. Sci.* **2023**, *10*, 1115746. [CrossRef]

24. Shin, D.; Song, S.; Ryoo, S.-B.; Lee, S.-S. Variations in Ozone Concentration over the Mid-Latitude Region Revealed by Ozonesonde Observations in Pohang, South Korea. *Atmosphere* **2020**, *11*, 746. [CrossRef]
25. Young, P.J.; Archibald, A.T.; Bowman, K.W.; Lamarque, J.-F.; Naik, V.; Stevenson, D.S.; Tilmes, S.; Voulgarakis, A.; Wild, O.; Bergmann, D.; et al. Pre-Industrial to End 21st Century Projections of Tropospheric Ozone from the Atmospheric Chemistry and Climate Model Intercomparison Project (ACCMIP). *Atmos. Chem. Phys.* **2013**, *13*, 2063–2090. [CrossRef]
26. Zeng, Y.; Zhang, J.; Li, D.; Liao, Z.; Bian, J.; Bai, Z.; Shi, H.; Xuan, Y.; Yao, Z.; Chen, H. Vertical Distribution of Tropospheric Ozone and Its Sources of Precursors over Beijing: Results from ~20 Years of Ozonesonde Measurements Based on Clustering Analysis. *Atmos. Res.* **2023**, *284*, 106610. [CrossRef]
27. Wang, T.; Xue, L.; Brimblecombe, P.; Lam, Y.F.; Li, L.; Zhang, L. Ozone Pollution in China: A Review of Concentrations, Meteorological Influences, Chemical Precursors, and Effects. *Sci. Total Environ.* **2017**, *575*, 1582–1596. [CrossRef]
28. Liu, Y.; Wang, T. Worsening Urban Ozone Pollution in China from 2013 to 2017—Part 2: The Effects of Emission Changes and Implications for Multi-Pollutant Control. *Atmos. Chem. Phys.* **2020**, *20*, 6323–6337. [CrossRef]
29. Yang, L.; Luo, H.; Yuan, Z.; Zheng, J.; Huang, Z.; Li, C.; Lin, X.; Louie, P.K.K.; Chen, D.; Bian, Y. Quantitative Impacts of Meteorology and Precursor Emission Changes on the Long-Term Trend of Ambient Ozone over the Pearl River Delta, China, and Implications for Ozone Control Strategy. *Atmos. Chem. Phys.* **2019**, *19*, 12901–12916. [CrossRef]
30. Hu, C.; Kang, P.; Jaffe, D.A.; Li, C.; Zhang, X.; Wu, K.; Zhou, M. Understanding the Impact of Meteorology on Ozone in 334 Cities of China. *Atmos. Environ.* **2021**, *248*, 118221. [CrossRef]
31. Bera, B.; Bhattacharjee, S.; Sengupta, N.; Saha, S. Variation and Dispersal of PM10 and PM2.5 during COVID-19 Lockdown over Kolkata Metropolitan City, India Investigated through HYSPLIT Model. *Geosci. Front.* **2022**, *13*, 101291. [CrossRef] [PubMed]
32. Tan, Z.; Lu, K.; Jiang, M.; Su, R.; Dong, H.; Zeng, L.; Xie, S.; Tan, Q.; Zhang, Y. Exploring Ozone Pollution in Chengdu, Southwestern China: A Case Study from Radical Chemistry to O3-VOC-NOx Sensitivity. *Sci. Total Environ.* **2018**, *636*, 775–786. [CrossRef] [PubMed]
33. Yu, S.; Su, F.; Yin, S.; Wang, S.; Xu, R.; He, B.; Fan, X.; Yuan, M.; Zhang, R. Characterization of Ambient Volatile Organic Compounds, Source Apportionment, and the Ozone–NO_X–VOC Sensitivities in a Heavily Polluted Megacity of Central China: Effect of Sporting Events and Emission Reductions. *Atmos. Chem. Phys.* **2021**, *21*, 15239–15257. [CrossRef]
34. Zavala, M.; Brune, W.H.; Velasco, E.; Retama, A.; Cruz-Alavez, L.A.; Molina, L.T. Changes in Ozone Production and VOC Reactivity in the Atmosphere of the Mexico City Metropolitan Area. *Atmos. Environ.* **2020**, *238*, 117747. [CrossRef]
35. Ou, S.; Wei, W.; Cheng, S.; Cai, B. Exploring Drivers of the Aggravated Surface O3 over North China Plain in Summer of 2015–2019: Aerosols, Precursors, and Meteorology. *J. Environ. Sci.* **2023**, *127*, 453–464. [CrossRef]
36. Li, K.; Jacob, D.J.; Liao, H.; Shen, L.; Zhang, Q.; Bates, K.H. Anthropogenic Drivers of 2013–2017 Trends in Summer Surface Ozone in China. *Proc. Natl. Acad. Sci. USA* **2019**, *116*, 422–427. [CrossRef]
37. Li, B.; Ho, S.S.H.; Li, X.; Guo, L.; Chen, A.; Hu, L.; Yang, Y.; Chen, D.; Lin, A.; Fang, X. A Comprehensive Review on Anthropogenic Volatile Organic Compounds (VOCs) Emission Estimates in China: Comparison and Outlook. *Environ. Int.* **2021**, *156*, 106710. [CrossRef]
38. Liang, X.; Sun, X.; Xu, J.; Ye, D. Improved Emissions Inventory and VOCs Speciation for Industrial OFP Estimation in China. *Sci. Total Environ.* **2020**, *745*, 140838. [CrossRef]
39. Jiang, Z.; Xiang, W.; Zhai, H.; Zheng, X.; Wang, Q.; Zhao, W.; Yin, Z. Variation Characteristics, Source Analysis, and Health Risk Assessment of Carbonyl Compounds in Zhangjiajie National Forest Park, China. *Atmos. Pollut. Res.* **2024**, *15*, 102029. [CrossRef]
40. Li, Y.; Li, H.; Zhang, X.; Ji, Y.; Gao, R.; Wu, Z.; Yin, M.; Nie, L.; Wei, W.; Li, G.; et al. Characteristics, Sources and Health Risk Assessment of Atmospheric Carbonyls during Multiple Ozone Pollution Episodes in Urban Beijing: Insights into Control Strategies. *Sci. Total Environ.* **2023**, *863*, 160769. [CrossRef]
41. Altshuller, A.P. Assessment of the Contribution of Chemical Species to The Eye Irritation Potential of Photochemical Smog. *J. Air Pollut. Control Assoc.* **1978**, *28*, 594–598. [CrossRef] [PubMed]
42. Liu, T.; Hong, Y.; Li, M.; Xu, L.; Chen, J.; Bian, Y.; Yang, C.; Dan, Y.; Zhang, Y.; Xue, L.; et al. Atmospheric Oxidation Capacity and Ozone Pollution Mechanism in a Coastal City of Southeastern China: Analysis of a Typical Photochemical Episode by an Observation-Based Model. *Atmos. Chem. Phys.* **2022**, *22*, 2173–2190. [CrossRef]
43. Salthammer, T. Formaldehyde in the Ambient Atmosphere: From an Indoor Pollutant to an Outdoor Pollutant? *Angew. Chem. Int. Ed.* **2013**, *52*, 3320–3327. [CrossRef]
44. Anderson, D.C.; Nicely, J.M.; Wolfe, G.M.; Hanisco, T.F.; Salawitch, R.J.; Canty, T.P.; Dickerson, R.R.; Apel, E.C.; Baidar, S.; Bannan, T.J.; et al. Formaldehyde in the Tropical Western Pacific: Chemical Sources and Sinks, Convective Transport, and Representation in CAM-Chem and the CCMI Models. *JGR Atmos.* **2017**, *122*, 11201–11226. [CrossRef] [PubMed]
45. Lü, H.; Cai, Q.-Y.; Wen, S.; Chi, Y.; Guo, S.; Sheng, G.; Fu, J. Seasonal and Diurnal Variations of Carbonyl Compounds in the Urban Atmosphere of Guangzhou, China. *Sci. Total Environ.* **2010**, *408*, 3523–3529. [CrossRef] [PubMed]
46. Li, Y.; Shao, M.; Lu, S.; Chang, C.-C.; Dasgupta, P.K. Variations and Sources of Ambient Formaldehyde for the 2008 Beijing Olympic Games. *Atmos. Environ.* **2010**, *44*, 2632–2639. [CrossRef]
47. Ling, Z.H.; Zhao, J.; Fan, S.J.; Wang, X.M. Sources of Formaldehyde and Their Contributions to Photochemical O3 Formation at an Urban Site in the Pearl River Delta, Southern China. *Chemosphere* **2017**, *168*, 1293–1301. [CrossRef]
48. Liu, D.; Wang, M.; Hu, K.; Liu, Z.; Dong, H.; Zhang, B.; Zhao, X.; Ji, W. Sources and Budget Analysis of Ambient Formaldehyde in the East-Central Area of the Yangtze River Delta Region, China. *Atmos. Environ.* **2023**, *305*, 119801. [CrossRef]

49. Su, W.; Liu, C.; Hu, Q.; Zhao, S.; Sun, Y.; Wang, W.; Zhu, Y.; Liu, J.; Kim, J. Primary and Secondary Sources of Ambient Formaldehyde in the Yangtze River Delta Based on Ozone Mapping and Profiler Suite (OMPS) Observations. *Atmos. Chem. Phys.* **2019**, *19*, 6717–6736. [CrossRef]
50. Duncan, B.N.; Yoshida, Y.; Olson, J.R.; Sillman, S.; Martin, R.V.; Lamsal, L.; Hu, Y.; Pickering, K.E.; Retscher, C.; Allen, D.J.; et al. Application of OMI Observations to a Space-Based Indicator of NOx and VOC Controls on Surface Ozone Formation. *Atmos. Environ.* **2010**, *44*, 2213–2223. [CrossRef]
51. Chen, Y.; Wang, M.; Yao, Y.; Zeng, C.; Zhang, W.; Yan, H.; Gao, P.; Fan, L.; Ye, D. Research on the Ozone Formation Sensitivity Indicator of Four Urban Agglomerations of China Using Ozone Monitoring Instrument (OMI) Satellite Data and Ground-Based Measurements. *Sci. Total Environ.* **2023**, *869*, 161679. [CrossRef] [PubMed]
52. Jung, J.; Choi, Y.; Mousavinezhad, S.; Kang, D.; Park, J.; Pouyaei, A.; Ghahremanloo, M.; Momeni, M.; Kim, H. Changes in the Ozone Chemical Regime over the Contiguous United States Inferred by the Inversion of NOx and VOC Emissions Using Satellite Observation. *Atmos. Res.* **2022**, *270*, 106076. [CrossRef] [PubMed]
53. Li, R.; Xu, M.; Li, M.; Chen, Z.; Zhao, N.; Gao, B.; Yao, Q. Identifying the Spatiotemporal Variations in Ozone Formation Regimes across China from 2005 to 2019 Based on Polynomial Simulation and Causality Analysis. *Atmos. Chem. Phys.* **2021**, *21*, 15631–15646. [CrossRef]
54. Ren, J.; Guo, F.; Xie, S. Diagnosing Ozone–NO_x–VOC Sensitivity and Revealing Causes of Ozone Increases in China Based on 2013–2021 Satellite Retrievals. *Atmos. Chem. Phys.* **2022**, *22*, 15035–15047. [CrossRef]
55. Witte, J.C.; Duncan, B.N.; Douglass, A.R.; Kurosu, T.P.; Chance, K.; Retscher, C. The Unique OMI HCHO/NO2 Feature during the 2008 Beijing Olympics: Implications for Ozone Production Sensitivity. *Atmos. Environ.* **2011**, *45*, 3103–3111. [CrossRef]
56. Zhan, Y.; Luo, Y.; Deng, X.; Grieneisen, M.L.; Zhang, M.; Di, B. Spatiotemporal Prediction of Daily Ambient Ozone Levels across China Using Random Forest for Human Exposure Assessment. *Environ. Pollut.* **2018**, *233*, 464–473. [CrossRef]
57. Li, M.; Cao, J.; Guo, J.; Niu, J.; Xiong, M. Response of Energy Consumption for Building Heating to Climatic Change and Variability in Tianjin City, China. *Meteorol. Appl.* **2016**, *23*, 123–131. [CrossRef]
58. Xie, H.; He, Y.; Xie, X. Exploring the Factors Influencing Ecological Land Change for China's Beijing–Tianjin–Hebei Region Using Big Data. *J. Clean. Prod.* **2017**, *142*, 677–687. [CrossRef]
59. Cedeno Jimenez, J.R.; Brovelli, M.A. NO_2 Concentration Estimation at Urban Ground Level by Integrating Sentinel 5P Data and ERA5 Using Machine Learning: The Milan (Italy) Case Study. *Remote Sens.* **2023**, *15*, 5400. [CrossRef]
60. Guanter, L.; Aben, I.; Tol, P.; Krijger, J.M.; Hollstein, A.; Köhler, P.; Damm, A.; Joiner, J.; Frankenberg, C.; Landgraf, J. Potential of the TROPOspheric Monitoring Instrument (TROPOMI) Onboard the Sentinel-5 Precursor for the Monitoring of Terrestrial Chlorophyll Fluorescence. *Atmos. Meas. Tech.* **2015**, *8*, 1337–1352. [CrossRef]
61. Iverson, L.R.; Graham, R.L.; Cook, E.A. Applications of Satellite Remote Sensing to Forested Ecosystems. *Landsc. Ecol.* **1989**, *3*, 131–143. [CrossRef]
62. *GB 3095-2012*; Environmental Air Quality Standards. China Environmental Science Press: Beijing, China, 2012.
63. Zheng, Z.; Yang, Z.; Wu, Z.; Marinello, F. Spatial Variation of NO_2 and Its Impact Factors in China: An Application of Sentinel-5P Products. *Remote Sens.* **2019**, *11*, 1939. [CrossRef]

Disclaimer/Publisher's Note: The statements, opinions and data contained in all publications are solely those of the individual author(s) and contributor(s) and not of MDPI and/or the editor(s). MDPI and/or the editor(s) disclaim responsibility for any injury to people or property resulting from any ideas, methods, instructions or products referred to in the content.